

**CHARACTERIZATION AND ALKALINE FUSION
RECOVERY PROCESS OF RARE EARTHS AND
THORIUM FROM MALAYSIAN MONAZITE**

SANJITH UDAYAKUMAR

UNIVERSITI SAINS MALAYSIA

2019

**CHARACTERIZATION AND ALKALINE FUSION RECOVERY PROCESS
OF RARE EARTHS AND THORIUM FROM MALAYSIAN MONAZITE**

by

SANJITH UDAYAKUMAR

**Thesis submitted in fulfillment of the
requirement for the degree of
Master of Science**

November 2019

ACKNOWLEDGEMENT

First and foremost, above all, God almighty is worthy of all the acknowledgements. This Master's thesis became a reality with the kind cooperation and support of many individuals. My heartfelt gratitude and thanks to all of them.

I wish to thank my supervisor Dr. Sheikh Abdul Rezan for his incredible effort to offer every possible help to finish this thesis. His valuable guidance, insightful discussions, scholarly advice helped me to successfully complete this research study. It was a great honor to complete this work under his supervision. My sincere thanks are due to him for all his help and support. My co-supervisors Prof. Ahmad Fauzi Bin Noor and Dr. Teuku Andika Rama Putra guided me throughout the research study. Prof. Ahmad Fauzi shared his experiences and provided the necessary moral support and Dr. Teuku Andika with his doctoral research experience, helped me to solve complicated problems mainly during my experiments. I thank them for their constructive ideas.

My thanks also are due to Dr. Sivakumar Ramakrishnan who has been my well-wisher and helped me in the statistical analysis of the different designs of experiments employed in this study. His supportive attitude and encouragement at every point during my research helped to overcome difficult moments. My appreciations to Dr. Norlia Baharun for mentoring and motivating me during my challenging phases of the research. I am indebted to Dr. Roshasnorlyza Hazan, Puan. Khaironie Mohd Takip, and Mr. Wilfred from Nuclear Malaysian Agency for helping me with crucial facilities and for their genuine kindness and invaluable help without any hesitation during the characterization and analysis of my research samples. I express my gratitude to the Dean Assoc. Prof. Dr. Syed Fuad B. Saiyid Hashim, former Dean Prof. Zuhailawati

Hussain, Prof. Dr. Khairunisak Bt. Abdul Razak, Prof. Dr. Ir. Mariatti Bt. Jaafar, Assoc. Prof. Dr. Kamar Shah B. Ariffin for their timely help and research motivation. Prof. Corby Anderson (Colorado school of mines, USA), Dr. Mark Pownceby (CSIRO, Australia) and Dr. Ismail Bin Ibrahim (Mineral Research Centre, Ipoh, Malaysia) provided me the opportunity to conduct my experiments and perform analysis via collaboration. I am thankful to them for their kind gesture.

This project was made possible by the financial support from Universiti Sains Malaysia (USM), Ministry of Education (MOE) of Malaysia and Malaysian Nuclear Agency (MNA). I am also gratefully acknowledging the financial support received from Institute of Post Graduate Studies through USM Fellowship, APEX. Main funding on this project was by USM Research University Individual (RUI) grant no: 1001/PBAHAN/814273 and USM Bridging grant (PBAHAN.6316116). Besides this, additional funding via MOE Fundamental Research Grant Scheme (FRGS) grant no: 203/PBAHAN/6071364 and FRGS grant no: 203.PBAHAN 6071402, with MNA Thorium flagship grant no: DSTIN FP0214D05-01 (DSTIN). Further support was by Nippon Sheet Glass Research Grant (NSGRG) (No. 304/PBAHAN/650360/N120).

Special thanks to USM technicians, Mr. Mohamad Shafiq Bin Mustapa Sukri, Mr. Mohammad Azrul Bin Zainol Abidin, Mr. Mohd. Helmi Bin Khir and Mr. Shahrul Ami Bin Zainal Abidin, Mr. Mohd Azam Bin Rejab, Mr. Kemuridan Bin Md. Desa, Mr. Muhammad Khairi Bin Khalid, Mr. Mohamad Hasnor Bin Husin, Mr. Zulkurnain Bin Hasbolah, Mr. Mohamad Zaini Bin Saari, Mr. Mokhtar Bin Mohamad and Puan Haslina Bt Zulkifli for their endless support in conducting, troubleshooting my experiments and analyzing my samples. My utmost thanks are due to them. I wish record my special thanks to Mr. Abdul Mutalib Bin Abdullah, Mr. Khairul Anuar, Mr. Ahmad Fadly Bin Jusoh and Mrs. Fatin for their extremely valuable support for

characterization studies of this project. I express my gratitude to Ms. Amira Sofea, of Science and Engineering Research Centre for supporting me in the ICP-MS analysis. The physical support and the technical contribution of the administrative staff of SMMRE and Institute of postgraduate studies, USM, were very kind and generous especially Mrs. Nur Shalydah, Mrs. Najmah binti Sabri and Mrs. Laila (Institute for Postgraduate Studies, Engineering campus) helped me more than just with paperwork.

My heart knows no bounds in expressing my cordial gratitude to Shaik Abdul Rahman and Shah Rizal, for being there during my tough times especially during the realization stage of my final thesis and helping me keep up with my progress. I'd also like to thank the members of metallurgy research team, Eltefat Ahmadi, Najwa Binti Ibrahim and Mohammad Rezaei for their contribution towards fruitful discussions regarding my project. My thanks to my friends, Ye Zarni Htwe, Anas, and Qummare Azam at Desa Utama, PG-5 family, the Postgraduate Student Club (PGSC, 2017-19) of School of Materials and Mineral Resources Engineering (SMMRE) and all the local and international postgrads in Engineering campus, USM for sharing their camaraderie. I acknowledge and cherish the company and encouragement of all my special friends Sharan, Anbalagan, Darwin, Laguneswary, Shafeeq and many more friends from Malaysia, towards the smooth completion of the project. Also, I wholeheartedly recognize the friendly advice and motivation of all my friends from Malaysia and India, especially SCABBDY, GM and Octas team. Their once in a while calls have made my pursuit feel very reinforced.

Last but not least, above ground, I am indebted to my parents, Dr. Udayakumar and Mrs. Sujatha Udayakumar, whose value to me only grows with age. I thank them for their never-ending support and all the sacrifices they have made on my behalf. They not only supported me financially but also extended their support morally and

emotionally. Special thanks to my mom's eternal prayers and dad's practical points of views. My gratitude is also extended to my uncle, Dr. Prem Kumar (Swins-i-Fosys), who has seldom failed to lift me up whenever I am emotionally down. My sister, Dr. U. Prithika Abhishek is the prime mover and the starting point of all the inspiration I acquired to pursue this research.

SANJITH UDAYAKUMAR

April 2019

TABLE OF CONTENTS

	Page
ACKNOWLEDGEMENT	ii
TABLE OF CONTENTS	vi
LIST OF TABLES	xii
LIST OF FIGURES	xv
LIST OF SYMBOLS	xxiv
LIST OF ABBREVIATIONS	xxvi
ABSTRAK	xxviii
ABSTRACT	xxx
CHAPTER ONE : INTRODUCTION	
1.1 Background of study	1
1.1.1 Occurrence of REE minerals	2
1.1.2 Principal REE minerals	6
1.1.3 Malaysian monazite – Potential source of REEs and Thorium	8
1.2 Problem statement	9
1.3 Objectives of the study	12
1.4 Scope of the research	13
1.5 Organization of thesis	14
CHAPTER TWO: LITERATURE REVIEW	
2.1 Introduction	16
2.2 Geological occurrence of monazite	17
2.3 Distribution of monazite sources in the world	18
2.3.1 Monazite: Global production	19
2.3.2 Monazite production in Malaysia	21
2.3.1 World reserves and production of REEs	22

2.4	Mineralogical variations of monazite	24
2.5	Applications of REEs of Monazite	26
2.6	Physical processing of monazite	29
2.7	Decomposition methods of monazite	30
2.7.1	Pyrometallurgical routes	34
2.7.2	Hydrometallurgical routes: Acidic and alkaline process	36
2.7.2 (a)	Effect of parameters on alkaline fusion	40
2.7.2 (b)	Effect of parameters on acidic leaching	42
2.7.3	Non-conventional methods	43
2.8	Separation and purification process for rare earths and recovery	43
2.9	Design of Experiments (DOE)	46
2.9.1	Taguchi approach of optimization	46
2.9.2	Fractional Factorial design	47
2.10	Summary	48
 CHAPTER THREE: MATERIALS AND METHODS		
3.1	Overview	50
3.2	Materials	53
3.3	Sample preparation	53
3.4	Raw material characterization	55
3.4.1	Visual and optical examination	55
3.4.2	SEM-EDX analysis	55
3.4.3	Particle size distribution	56
3.4.4	XRD studies	56
3.4.5	FTIR analysis	58
3.4.6	XRF analysis	58
3.4.7	Automated mineralogy	60
3.4.8	EPMA analysis	61

3.4.9	Inductively coupled plasma mass spectrometry (ICP-MS)	62
3.4.10	Loss on ignition test	58
3.4.11	TGA-DTA analysis	63
3.5	Experimental Methodology	63
3.5.1	High temperature carbothermal dephosphorization of Malaysian monazite	63
3.5.1 (a)	Experimental setup	65
3.5.1 (b)	Optimization of dephosphorization behavior using Taguchi Approach	68
3.5.2	Alkaline fused-water leaching process	70
3.5.3	Acidic leaching of REE and Th hydrous oxides	73
3.5.4	Fractional factorial design for alkaline fusion and acid leaching	74
3.5.5	Experimental setup	77

CHAPTER FOUR: RESULTS AND DISCUSSION

4.1	Introduction	82
4.2	Characterization of Malaysian monazite concentrates	84
4.2.1	Monazite occurrence in Ipoh	84
4.2.2	Visual assessment of the monazite concentrates	85
4.2.3	Optical analysis	86
4.2.4	Loss on ignition (LOI)	90
4.2.5	XRF analysis	91
4.2.6	Inductive coupled plasma-mass spectrometry	94
4.2.7	X-ray diffraction studies	98
4.2.8	Advanced mineral identification and characterization system (AMICS)	101
4.2.9	Electron probe micro-analysis (EPMA)	103
4.2.10	Particle size analysis (PSA)	107

4.2.11	Morphological and elemental analysis	108
4.2.12	Fourier transform infrared absorption (FTIR) studies:	120
4.2.13	Thermogravimetric and differential thermal analysis (TGA-DTA)	122
4.3	High temperature carbothermal dephosphorization of monazite	125
4.3.1	Thermodynamic analysis of dephosphorization	126
4.3.2	Equilibrium composition diagram of dephosphorization	132
4.3.3	XRD analysis of decomposition of raw monazite	137
4.3.4	Analysis of dephosphorization behaviour of Malaysian monazite	140
4.3.5	Analysis of signal to noise (S/N) ratio	142
4.3.6	Validation test	145
4.3.7	Microstructural characterization of dephosphorized products	145
4.4	Alkaline fusion of Malaysian monazite	151
4.4.1	Thermodynamics of formation of rare earth and thorium hydroxide-oxides from monazite concentrate by alkaline fusion	155
4.4.2	Feasibility analysis of formation of RE and Th hydroxide and oxide from monazite	159
4.4.3	DOE analysis	161
4.4.4	Removal of phosphorous and silicon by alkaline fusion process	162
4.4.5	Analysis of variance	165
4.4.6	Main effects and interactions	168
4.4.7	XRD analysis of REE hydroxide-oxide	175
4.4.8	Effect of parameters on phase transformation of water leach products	181
4.4.8 (a)	Effect of fusion temperature	181
4.4.8 (b)	Effect of fusion time	183
4.4.8 (c)	Effect of ratio of sodium hydroxide to monazite	185
4.4.8 (d)	Effect of particle size	187

4.4.9	Morphological analysis by SEM-EDX	189
4.4.10	Recovery of rare earths and Thorium after alkali-fused water leaching	191
4.5	Evaluation of high temperature and low temperature pyrometallurgical process for decomposition of monazite	192
4.6	Acidic leaching of rare earth and thorium hydroxides and oxides	196
4.7	Thermodynamics of formation of rare earth and thorium chlorides from REE and thorium hydroxide-oxides	197
4.8	Recovery of REE's and thorium	203
4.8.1	DOE analysis	204
4.8.2	ANOVA: Acid leaching	208
4.8.3	Main effects and interactions	211
4.8.4	Microstructural characterization of undigested solid by XRD analysis	218
4.8.5	Effect of factors of acid leaching	221
4.8.5 (a)	Effect of leaching temperature and leaching time	221
4.8.5 (b)	Effect of leaching time	223
4.8.5 (c)	Effect of ratio of solid to liquid	224
4.8.5 (d)	Effect of stirring speed	225
4.8.6	Morphological analysis of undigested solid	226
4.8.7	Behaviour of impurities during alkaline fused-water leaching	228
4.8.8	Improvement of REE and thorium recovery by modified diagnostic acid leaching	229
4.9	Alkaline fused-acid leach process - Summary	238
CHAPTER FIVE: CONCLUSIONS AND RECOMMENDATIONS		
5.1	Conclusions	239
5.2	Recommendations	243

REFERENCES

244

APPENDICES

Appendix A

Appendix B

Appendix C

Appendix C

Appendix C

Appendix D

Appendix E

Appendix F

Appendix G

Appendix H

Appendix I

Appendix J

Appendix K

Appendix L

Appendix M

Appendix N

Appendix O

LIST OF PUBLICATIONS

LIST OF TABLES

	Page
Table 1.1: Selected major REE bearing minerals in the world	4
Table 1.2: Thorium concentration ppm of various minerals	5
Table 2.1: Comparison of rare earth fraction and thorium concentration in monazite from different locations	20
Table 2.2: Production of rare earth minerals in Malaysia from 2014-17	22
Table 2.3 : Estimated world mine production of rare earth oxides and reserves	22
Table 2.4: Distribution of REEs by End Use in 2008	26
Table 2.5: Rare Earth Elements, Their Applications.	28
Table 2.6: Monazite and Xenotime Cracking methods	33
Table 2.7: Commercially used extractants for rare earth solvent extraction	45
Table 3.1: Raw materials and chemicals: Specifications and purpose.	53
Table 3.2: Experimental parameters and their levels.	69
Table 3.3: Orthogonal array for Taguchi design (3^3)	70
Table 3.4: Design of experiments for alkali fusion: Parameters and levels	75
Table 3.5: Design of experiments for acidic leaching: Parameters and levels	75
Table 3.6: DOE Table: Alkaline fusion experiment	76
Table 3.7: DOE Table: Acid leaching experiment using 6M HCl.	76
Table 4.1: Determination of LOI percent (%).	91

Table 4.2: Comparison of chemical composition of monazite using different sample preparation and characterization methods.	92
Table 4.3: AMICS quantitative mineralogical results.	102
Table 4.4: Modal analysis results from the phase-patched map	104
Table 4.5: Infrared transmission bands of Malaysian monazite.	121
Table 4.6: Relationship between Gibbs free Energy (ΔG , kJ/mol) and Equilibrium temperature (T_{eq} , °C) for possible reactions of different phases of monazite with graphite.	135
Table 4.7: Taguchi L9 (3^3) experimental plan, parameters, and results.	140
Table 4.8: Response table for means.	143
Table 4.9: DOE Table and responses: Alkaline fused water leaching.	162
Table 4.10: Analysis of variance (ANOVA) for the regression model of (a) percent phosphorous removal (X_P) obtained from alkaline-fused water leaching of Malaysian monazite.	166
Table 4.11: Statistical parameters for the response in Alkaline fused water leaching.	166
Table 4.12: Weighted R-profile and GoF values for different phases obtained from Rietveld refinement (ND= not detectable).	178
Table 4.13: Confirmatory analysis of REE and Th recovery by chemical analysis of Na_3PO_4 filtrate.	191

Table 4.15: Analysis of variance (ANOVA) for the regression model of percent REE and Th recovered obtained from acid leaching of REE and Th hydrous oxide mixture.	209
Table 4.16: Statistical parameters for the response in Acid Leaching	209
Table 4.17: Weighted R-profile and GoF values for different phases in the undigested solid from acid leaching obtained from Rietveld refinement.	220
Table 4.18: Recovery of REEs and Th for improved conditions.	235
Table 4.19: Elemental concentrations at different spots and areas of undigested solid obtained after 30 wt.% H ₂ O ₂ addition in 6M HCl.	237

LIST OF FIGURES

	Page
Figure 1.1: Distribution of primary and secondary REE deposits across the globe	3
Figure 2.1: Diversity of applications of Rare Earth Elements.	24
Figure 2.2: REE production by different countries and utilization for different applications in 2017	27
Figure 2.4: Typical separation flowsheet for REE from bastnäsité and monazite.	44
Figure 3.1: Overall process flow chart of the research work	52
Figure 3.2: Experimental set-up of high temperature carbothermal dephosphorization.	66
Figure 3.3: Flow chart for high temperature carbothermal dephosphorization of Malaysian monazite	67
Figure 3.4: Crucible in the box-furnace (left) and water leaching set-up (right)	78
Figure 3.5: Experimental setup for acid leaching using 6M HCl for dissolution of REEs and Th.	80
Figure 3.6: Overall methodology of alkaline fused water leaching and acid leaching for the recovery of REEs and Th.	81
Figure 4.1: Raw monazite concentrate separated from heavy mineral sands.	86
Figure 4.2: Different grains of monazite concentrate under optical microscope for different magnifications (100x, 50x).	88
Figure 4.3: Comparison of dry chemical analysis (XRF) for powder pressed and fused bead Malaysian monazite.	94

Figure 4.4: Comparison of wet chemical analysis (ICP-MS) for microwave digested and Lithium tetraborate fused-digested Malaysian monazite.	96
Figure 4.5: Comparison of elemental composition of Malaysian monazite using wet and dry chemical analysis.	97
Figure 4.6: X-ray diffraction spectrum of raw Malaysian monazite concentrate.	99
Figure 4.8: (a and c) Backscattered images of as received and powdered sample; (b and d) Identified minerals of as received and powdered sample.	103
Figure 4.9: Clustered and phase-patched map results for the monazite sample. Only phases with an area percent >0.1% are shown	105
Figure 4.10: Density-based scatter plots from each pixel within the mapped area showing the concentration (expressed as an elemental k-ratio) for the elements: a) Ce, b) La and c) Nd plotted against Th.	106
Figure 4.11: Size distribution of Malaysian monazite concentrate (as received).	108
Figure 4.12: Scanning electron micrographs of ground monazite concentrate. (Zrn-Zircon, Mnz-Monazite, Ilm- Ilmenite, Sil-Sillimanite)	110
Figure 4.13: Isolated grain backscattered images of monazite concentrate with their EDX spectrum; (a) monazite grain with Fe-Nb; (b) zircon; (c) ilmenite; (d) Fused zircon-monazite grain; (e) Ca-inclusion in monazite; (f) monazite with zircon-type structure.	113
Figure 4.14: Scanning electron microscope images and EDX mapping of isolated monazite grain	116
Figure 4.15: Scanning electron microscope images and EDX mapping of monazite concentrate.	117

Figure 4.16: Scanning electron microscope images and EDX mapping of Fe, Ti, S inclusions in monazite concentrate.	118
Figure 4.17: Scanning electron microscope images and EDX mapping of xenotime interlocked in monazite grain	119
Figure 4.18: Infrared spectrum of Malaysian monazite concentrates.	120
Figure 4.19: TG-DTA curves of Malaysian monazite concentrate.	123
Figure 4.20: Gibbs free energy diagram for decomposition reaction of monazite.	124
Figure 4.21: Photographs of the initial and final during different stages of the dephosphorization. a) Pressed pellet of monazite and graphite b) mixture of monazite and graphite before pelletization, c) distorted shape of pellet post dephosphorization, d) reacted and unreacted portion of monazite graphite post dephosphorization.	125
Figure 4.22: Predominance diagram for monazite system (Ce, La, Nd, Th-P-O system) for reducing conditions.	127
Figure 4.23: TG-DTA analysis of a) raw monazite and b) dephosphorization reaction of monazite with graphite.	129
Figure 4.24: Reaction feasibility for dissociation of CePO_4 into Ce_2O_3 and X (X = P_2O_5 , $\text{P}_2\text{O}_5(\text{g})$, $\text{PO}(\text{g})$, $\text{PO}_2(\text{g})$, $\text{P}_4\text{O}_6(\text{g})$ and $\text{P}(\text{g})$).	131
Figure 4.25: Reaction feasibility for dissociation of LaPO_4 into La_2O_3 and X (X = P_2O_5 , $\text{P}_2\text{O}_5(\text{g})$, $\text{PO}(\text{g})$, $\text{PO}_2(\text{g})$, $\text{P}_4\text{O}_6(\text{g})$ and $\text{P}(\text{g})$).	131
Figure 4.26: Reaction feasibility for dissociation of NdPO_4 into Nd_2O_3 and X (X = P_2O_5 , $\text{P}_2\text{O}_5(\text{g})$, $\text{PO}(\text{g})$, $\text{PO}_2(\text{g})$, $\text{P}_4\text{O}_6(\text{g})$ and $\text{P}(\text{g})$).	132

Figure 4.27: Equilibrium composition of reaction products formed for reactant interactions occurring for different molar ratios of phases of monazite (CePO_4 , Ce_2O_3 , CeO_2 , LaPO_4 and NdPO_4) to graphite (C).	136
Figure 4.28: XRD patterns of raw monazite at different temperatures	139
Figure 4.29: Main effects plot for dephosphorization.	144
Figure 4.30: Interaction effects plot for dephosphorization.	144
Figure 4.31: Morphology images of mixture of monazite concentrate and graphite (a) before and (b) after dephosphorization.	146
Figure 4.32: SEM-EDX of selected samples (a) HTD8 (b) HTD3 (c) HTD Best (d) HTD Best-Before dephosphorization.	147
Figure 4.33: Comparison of FTIR of dephosphorized products with Raw monazite concentrate.	148
Figure 4.34: Comparison of XRD patterns of selected dephosphorized samples with raw monazite concentrate.	149
Figure 4.35: Photographic images of alkaline fused monazite concentrate for different temperatures.	153
Figure 4.36: Photographic images of water leached samples after fusion at different conditions.	154
Figure 4.37: Solid REE hydroxide-oxide particles with undigested monazite after filtration of water leach solution.	155
Figure 4.38: Solid tri-sodium phosphate (Na_3PO_4) crystallized in the filter paper containing REOs and $\text{RE}(\text{OH})_3$	155

Figure 4.39: Eh–pH diagrams for the Th–, Nd–, Ce–, La–PO ₄ –H ₂ O systems at 25 °C, {PO ₄ }=10 ⁻³ M: (a) {Th}=10 ⁻³ M, (b) {Nd}=10 ⁻³ M, ΔG ^o _{NdPO₄}=–423.46 kcal/mol, (c) {Ce}=10⁻³ M, ΔG^o_{CePO₄}=–421.75 kcal/mol, (d) {La}=10⁻³ M, ΔG^o_{LaPO₄}=–425.78 kcal/mol.}}}	157
Figure 4.40: Eh–pH diagrams for the Th–, Nd–, Ce–, La–H ₂ O systems at 25 °C: (a) {Th}=10 ⁻³ M, (b) {Nd}=10 ⁻³ M, (c) {Ce}=10 ⁻³ M, (d) {La}=10 ⁻³ M.(Kim et al., 2012).	158
Figure 4.41: Gibbs free energy diagram for possible reaction pathways in alkaline fusion of monazite.	160
Figure 4.42: Ratio of weight of fused solid after fusion to weight of solid before fusion.	163
Figure 4.43: Percent weight loss of solid after water leaching to solid before fusion (%).	164
Figure 4.44: Relational analysis of weight loss percent of solid before fusion and solid after water leaching with % X _p and %X _{Si} .	164
Figure 4.45: Predicted versus actual values for percent removal of phosphorous	167
Figure 4.46: Equation for regression model: Percent removal of phosphorous (X _p)	168
Figure 4.47: Main effects plot fo percent removal of (a) P (X _p).	169
Figure 4.48: Standardized effects of different process parameters of alkaline fusion for percent removal of phosphorous (X _p) as response	169

Figure 4.49: The interaction plots for percent removal of phosphorous (X_p) as a function of fusion temperature, fusion time, ratio of NaOH to monazite and particle size.	171
Figure 4.50: Contour plots for the interaction effect of process parameters of alkaline fusion on percent removal of phosphorous (X_p).	174
Figure 4.51: Comparison of XRD spectrum of solid residue of best fusion condition (350°C, 4 hours, NaOH to monazite :4, 50 μ m particle size) and raw monazite before fusion.	176
Figure 4.52: XRD spectra of the solid residue obtained after water leaching for different fusion conditions in the DOE.	177
Figure 4.53: Comparison of XRD of water leach products between higher and lower fusion temperature conditions.	183
Figure 4.54: Comparison of XRD of water leach products between higher and lower fusion time conditions.	185
Figure 4.55: Comparison of XRD of water leach products between higher and lower fusion ratio of NaOH to monazite.	187
Figure 4.56: Comparison of XRD of water leach products between higher and lower particle sizes of raw monazite.	188
Figure 4.57: SEM-EDX of water leach products for the best fusion condition (BFC), highest (R9), lowest (R3) values of X_p and raw monazite.	190
Figure 4.58: In-situ XRD analysis of alkaline fusion dephosphorized monazite with NaOH	194
Figure 4.59: Insitu XRD analysis of alkaline fusion of raw monazite with NaOH	196
Figure 4.60: Eh-pH diagram of Ce-Cl-H ₂ O system at 90 °C and Gibbs free	199

energy diagram for feasibility of reactions during acid leaching.	
Figure 4.61: Eh-pH diagram of Th-Cl-H ₂ O system at 90 °C and Gibbs free energy diagram for feasibility of reactions during acid leaching.	200
Figure 4.62: Eh-pH diagram of Nd-Cl-H ₂ O system at 90 °C and Gibbs free energy diagram for feasibility of reactions during acid leaching.	201
Figure 4.63: Eh-pH diagram of La-Cl-H ₂ O system at 90 °C and Gibbs free energy diagram for feasibility of reactions during acid leaching.	202
Figure 4.64: Weight percent of solid (% W _{dig}) digested using 6M HCl leaching.	204
Figure 4.65: REE and Th recovered (% R _{total}) using 6M HCl leaching.	206
Figure 4.66: Weight percent of solid digested compared with percent recovery of Ce, La, Nd and Th during 6M HCl leaching.	207
Figure 4.67: Predicted versus actual values for percent recovery of REEs and Th (%).	210
Figure 4.68: Equation for regression model: Percent recovery of REEs and Th (%)	210
Figure 4.69: Standardized effects of different process parameters of acid leaching for percent recovery of REEs and Th (%) as response.	211
Figure 4.70: Main effects plot for percent recovery of Ce (% R _{Ce}) as a function of leaching temperature, leaching time, ratio of solid to liquid and stirring speed.	212
Figure 4.71: Main effects plot for percent recovery of Th (% R _{Th}) as a function of leaching temperature, leaching time, ratio of solid to liquid and stirring speed.	213

Figure 4.72: Main effects plot for percent recovery of La ($\% R_{La}$) as a function of leaching temperature, leaching time, ratio of solid to liquid and stirring speed.	213
Figure 4.73: Main effects plot for percent recovery of Nd ($\% R_{Nd}$) as a function of leaching temperature, leaching time, ratio of solid to liquid and stirring speed.	214
Figure 4.74: The interaction plots for percent removal of phosphorous (X_p) as a percent recovery of Ce (R_{Ce}), as a function of leaching temperature, leaching time, ratio of solid to liquid and stirring speed	215
Figure 4.75: The interaction plots for percent removal of phosphorous (X_p) as a percent recovery of Th (R_{Th}), as a function of leaching temperature, leaching time, ratio of solid to liquid and stirring speed	215
Figure 4.76: The interaction plots for percent removal of phosphorous (X_p) as a percent recovery of Nd (R_{Nd}) as a function of leaching temperature, leaching time, ratio of solid to liquid and stirring speed	216
Figure 4.77: The interaction plots for percent removal of phosphorous (X_p) as a percent recovery of La (R_{La}), as a function of leaching temperature, leaching time, ratio of solid to liquid and stirring speed	216
Figure 4.78: Contour plots for the interaction effect of process parameters of acid leaching on percent recovery of REEs and Th ($\% R_{total}$)	217
Figure 4.79: XRD spectra of the undigested residue obtained after 6M HCl leaching for different acid leaching conditions in the DOE.	219
Figure 4.80: Comparison of XRD of undigested solid after acid leaching between higher and lower leaching temperatures.	222

Figure 4.81: Comparison of XRD of undigested solid after acid leaching between higher and lower leaching times.	223
Figure 4.82: Comparison of XRD of undigested solid after acid leaching for higher and lower solid to liquid ratios.	224
Figure 4.83: Comparison of XRD of undigested solid after acid leaching between higher and lower stirring speeds	226
Figure 4.84: SEM analysis of morphology of acid leach residue with highest RE recovery (AL 10).	227
Figure 4.85: SEM analysis of morphology of acid leach residue with lowest RE recovery (AL3).	228
Figure 4.86: Amount of Y and Zr present in acid leach filtrate.	229
Figure 4.87: Wet air oxidation $(\text{OH})_3$ conversion to Ce (IV) oxide -wet oxidation kinetics. Data from (Zou et al., 2014).	230
Figure 4.88: Change of solution colour after addition of 30 wt. % H_2O_2 from (a) dark brown to (b) dirty white. (c) Undigested solid obtained for 6M HCl for 6 hours leaching time, 90°C and 300 rpm. (d) Undigested solid obtained with addition of 30 wt. % H_2O_2 in the acid leach mixture.	234
Figure 4.89: SEM images of undigested solid obtained with addition of 30 wt. % H_2O_2 in 6M HCl acid	236

LIST OF SYMBOLS

D_{v50}	Average particle size or median diameter
Z	Atomic numbers
cm	Centimeter
ΔG°	Change in Gibb's free Energy
C.V.	Coefficient of Variation
R^2	Correlation coefficient
$^\circ\text{C}$	Degree Celsius
T_{eq}	Equilibrium temperature
P_f	Final amount of phosphorus
F value	Fisher value
v	Frequency
GoF	Goodness of Fit
g	Gram
g/L	Gram per litre
h	hour
P_i	Initial amount of phosphorus
kJ/mol	Kilojoule per mole
kV	Kilovolt
kW	Kilowatt
μm	Micrometer
msec	milli seconds
mg	Milligram
ml	Milliliter
mm	millimeter
Min	Minute

M	Molar
nA	Nanoampere
%	Percent
D _p	Percent dephosphorization
X _p	Percent removal of phosphorous
X _{Si}	Percent removal of Silicon
S/N	Signal to Noise Ratio
R _{total}	Total recovery percentage
TBP	Tributyl phosphate
wt. %	Weight percent
R _{wp}	Weighted Profile R-factor

LIST OF ABBREVIATIONS

AAS	Atomic Absorption Spectrophotometer
AMICS	Advanced Mineral Identification and Characterization System
ANOVA	Analysis of variance
BSE	Back-scattered Electron
DI	Deionized
DOE	Design of Experiment
DTA	Differential Thermal Analysis
ED	Energy Dispersive
EDS	Energy Dispersive X-ray Spectroscopy
EDX	Energy Dispersive X-ray Spectroscopy
EPMA	Electron Probe Micro Analyzer
FESEM	Emission Scanning Electron Microscopy
FTIR	Fourier Transform Infrared Spectroscopy
HREE	Heavy Rare Earth Elements
HTCTD	High Temperature Carbothermal Dephosphorization
ICP	Inductively Coupled Plasma
ICP-MS	Inductive Couple Plasma Mass Spectrometry
ICP-OES	Inductive Couple Plasma Optical Emission Spectrometry
IUPAC	International Union of Pure and Applied Chemistry
LOI	Loss on ignition
LREE	Light Rare Earth Elements
MLA	Mineral liberation Analysis
NORE	Naturally Occurring Radioactive Elements
NREE	Naturally Occurring Radioactive Elements
OM	Optical Microscopy

ppb	Part per billion
ppm	Part per million
ppt	Part per thousand
PSA	Particle Size Analysis
PVA	Polyvinyl Alcohol
QXRD	Quantitative X-ray Diffraction
R&D	Research and development
RE	Rare Earth
REE	Rare Earth Elements
REO	Rare Earth Oxide
REP	Rare Earth Phosphates
rpm	Rotation per minute
SEM	Scanning Electron Microscopy
STA	Simultaneous Thermal Analyzer
TGA	Thermogravimetric Analysis
TPP	Temperature Partial Pressure
USGS	United States Geological Survey
WD	Wavelength Dispersive
WD-XRF	Wavelength Dispersive X-Ray Fluorescence Spectrometer
XRD	X-ray Diffraction
XRF	X-ray Fluorescent Spectroscopy

PENCIRIAN DAN PROSES PEROLEHAN PELAKURAN ALKALI TERHADAP UNSUR-UNSUR NADIR BUMI DAN TORIUM DARIPADA MONAZIT MALAYSIA

ABSTRAK

Perolehan unsur-unsur nadir bumi (REE) dan Torium (Th) daripada monazit Malaysia melalui kaedah pelakuran alkali dan pelarutlesapan asid yang mesra alam telah dikaji dalam penyelidikan ini. Sebelum pemprosesan monazit beralkali, pencirian kimia dan mineralogi yang mendalam terhadap monazit Malaysia telah dijalankan dalam kajian ini. Kajian pencirian konsentrat yang sistematik telah dikendalikan menggunakan teknik-teknik seperti Mikroskopi Optik (OM), Mikroskopi Elektron Pensakan (SEM) yang dilengkapi dengan Spektroskopi Penyebar Tenaga Sinar-X (EDS) dan Spektroskopi Inframerah Transformasi Fourier (FTIR). Teknik-teknik ini menganalisis morfologi permukaan yang teripinci, analisis unsur, penilaian persekutuan mineral dan identifikasi permukaan kumpulan berfungsi. Analisis XRF bagi komposisi pukal mengesahkan kehadiran Ce, La, Nd, Pr dan Y (~ 70 % berat REE) manakala torium menyumbang sebanyak 7 % daripada berat komposisi total. Keputusan analisis XRD telah mengesahkan konsentrat itu terdiri terutamanya daripada monazit (Ce, La, Nd, Th (PO₄)) berserta fasa-fasa kuarza yang minimum. Kajian penyahfosforus karboterma bersuhu tinggi (HTCTD) telah dijalankan bagi menilai tingkah laku penguraian mineral fosfat di bawah pengaruh suhu, saiz partikel dan nisbah molar monazit kepada karbon yang berbeza. Tanpa mengambil kira perbezaan keadaan bagi penurunan karboterma, 97 % penyahfosforus telah berjaya dicapai dalam kajian ini. Keadaan optimal bagi penyahfosforus telah dirumuskan pada suhu penurunan 1350 °C, saiz partikel 75 µm dan nisbah molar monazit kepada karbon sebanyak 0.3. Kaedah baru dalam pemprosesan beralkali telah

diuji dalam penyelidikan. Melalui kaedah ini, kesan suhu lakuran ($350 - 450\text{ }^{\circ}\text{C}$), masa ($2 - 4$ jam), nisbah berat monazit kepada alkali (NaOH) ($2 - 4$), dan saiz partikel (-50 , -100 , $-150\text{ }\mu\text{m}$) terhadap penguraian monazit telah dikaji menggunakan pecahan reka bentuk faktor eksperimen di peringkat pelakuran alkali. Peratus penyingkiran tertinggi bagi fosforus (X_p) dan silikon (X_{Si}) telah diperolehi pada suhu lakuran $350\text{ }^{\circ}\text{C}$, masa lakuran 4 jam, nisbah berat monazit kepada natrium hidroksida sebanyak 4 , dan saiz partikel terendah yang diuji dalam kajian ini, iaitu $-50\text{ }\mu\text{m}$. Pencernaan asid bagi oksida berhidrat yang diperolehi daripada peringkat pelarutlesapan air berlakur dengan kondisi yang terbaik telah dijalankan menggunakan asid hidroklorik bermolar 6 bagi memperoleh REE dan Th dalam larutan nadir bumi berklorida (RECl_3). Berdasarkan parameter-parameter yang telah dikaji seperti suhu pelarutlesapan ($70 - 90\text{ }^{\circ}\text{C}$), masa pelarutlesapan ($30 - 90$ minit), nisbah pepejal kepada cecair ($20 - 40\text{ g/L}$) dan kelajuan adukan ($300 - 700\text{ rpm}$), perolehan yang rendah sebanyak 12% dan kurang telah dicapai disebabkan ciri-ciri termodinamik REO dan Th yang stabil. Oleh itu, pengubahsuaian kaedah pelarutlesapan asid menggunakan hidrogen peroksida (H_2O_2) telah dicadangkan untuk meningkatkan kadar perolehan. Tanpa penggunaan H_2O_2 , perolehan REOs telah dicapai sebanyak 18.14% manakala dengan penggunaan H_2O_2 , perolehan berjaya ditingkatkan kepada 63.78% .

CHARACTERIZATION AND ALKALINE FUSION RECOVERY PROCESS OF RARE EARTHS AND THORIUM FROM MALAYSIAN MONAZITE

ABSTRACT

The recovery of rare earth elements (REEs) and thorium (Th) from Malaysian monazite through an environmental-friendly alkali-fused and acid leached method was investigated in this research. Prior to the alkaline processing of monazite, an in-depth chemical and mineralogical characterization of Malaysian monazite, from Ipoh, Perak, Malaysia was conducted in the study. A systematic characterization study of the concentrate was conducted using Optical Microscopy (OM), Scanning Electron Microscopy (SEM) equipped with Energy Dispersive X-ray Spectroscopy (EDS) and Fourier Transform Infrared Spectroscopy (FTIR). These techniques analyzed the morphological details on the surface, elemental analysis, mineral association assessment and identification of the surface functionalization groups. The XRF analysis for bulk composition confirmed the presence of Ce, La, Nd, Pr and Y (REE's ~70 wt. %) while Th accounted for 7 wt. % of the total composition. The XRD results confirmed that the concentrate was primarily composed of monazite (Ce, La, Nd, Th (PO₄)) along with minor impurity phases of quartz. High temperature carbothermal dephosphorization (HTCTD) was performed to assess the decomposition behavior of the phosphate mineral under different conditions of temperature, particle size and monazite to carbon ratio. At all the conditions investigated for carbothermal reduction, up to 97 % dephosphorization was achieved in the study. The optimal condition attained 97.85 % dephosphorization for a reduction temperature of 1350°C, particle size fraction of -75 μm and monazite to carbon molar ratio of 0.3. A new alkaline fusion method was explored in this research. In this method, the effects of fusion

temperature (350-450 °C), fusion time (2-4 hrs), weight ratio of monazite to alkali (NaOH) (2-4), and particle size fractions (-50 to -150 μm) on the decomposition of monazite were investigated using fractional factorial design (FFD) of experiments for the alkaline fusion stage. The highest percent removal of phosphorous (X_p) i.e., 95.02 % and silicon (X_{si}) i.e., 75.82 % was obtained for a fusion temperature of 350°C, fusion time of 4 hours, weight ratio of monazite to NaOH of 4, and the lowest particle size studied in this work i.e, 50 μm. Acid digestion of the hydrous oxides obtained from the best condition for fused-water leaching stage was conducted using 6M HCl for recovering the REE and Th in form of soluble rare earth chlorides ($RECl_3$). Of the parameters investigated, such as leaching temperature (70-90°C), leaching time (30-90 minutes), solid to liquid ratio (20-40 g/L) and stirring speed (300-700 rpm), low recovery i.e., 12 % and below, was achieved due to the stable thermodynamic behavior of the REOs and Th. Therefore, a modification of the acid leaching method with the use of hydrogen peroxide (H_2O_2) was proposed to enhance recovery. Without H_2O_2 , the recovery of REOs was 18.14 % whereas with H_2O_2 assisted leaching, the recovery improved to 63.78 %.

CHAPTER ONE

INTRODUCTION

1.1 Background of study

The fifteen lanthanide elements in the periodic table along with scandium and yttrium distributed over 250 different minerals are designated as rare earth elements (REE's), i.e., with atomic numbers, $Z = 57$ (lanthanum, La) to 71 (lutetium, Lu), together with yttrium (Y, $Z= 39$) and scandium (Sc, $Z= 21$). Generally, scandium (Sc) and yttrium (Y) are also included in this category as their occurrence is associated with the same ore deposits as the lanthanides and they exhibit similar chemical properties (Castor and Hedrick, 2006). This particular group of elements has been recognized as critical and rare, as the natural occurrence of these elements is greatly dependent on the geological conditions, wherein they are only found in sufficient concentrations and amounts in few regions, in economically viable and exploitable forms (Kanazawa and Kamitani, 2006; Balaram, 2019). The conventional manner of distinguishing the rare earth elements (REE) is by means of their atomic numbers, where lower atomic weight elements from lanthanum to samarium (Sm) are referred to as the light rare earth elements (LREE); while europium (Eu) to lutetium, are the heavy rare earth elements (HREE). Yttrium is grouped with the heavy rare earth elements due to their chemical similarities (Jones et al., 1995).

Most of the REEs are not as rare in nature as the name implies. It is mostly treated as a historical misnomer because the term 'rare earths' reflect unfamiliarity rather than truly rare nature of their existence. On the contrary, the REE's are considerably ample in the Earth's crust with an overall abundance of 9.2 ppm in the Earth's crust. On an average, with respect to the proportion of the Earth's continental

crust, the most abundant REE is Cerium (Ce) at 43 parts per million (ppm) and the rarest REE is thulium (Tm, 0.28 ppm), excepting promethium (Pm) which is virtually absent, because of the short half-life due to its radioactivity. Lanthanum (La) and neodymium (Nd) followed cerium amounting to about 20 ppm while, yttrium occurs at 19 ppm (Wedepohl, 1995; Rudnick and Gao, 2003). Thus, their overall abundances are not disparate from many other important elements such as lithium (17 ppm), germanium (1.3 ppm), copper (27 ppm), lead (11 ppm), tin (1.7 ppm), and uranium (1.3 ppm) (Taylor and McLennan, 1985). Due to the larger ionic radii of the lighter REEs, they tend to occur more concentrated in the continental crust than the larger atomic number REEs. The resemblances in the chemical nature (oxidation states and ionic radii) of the REEs permit them to substitute for one another in crystal structures as a result of which multiple REEs occur within a single mineral and a wide distribution in the Earth's crust. Furthermore, the slight chemical and physical dissimilarities within the REEs are due to the small differences in ionic radius which results in segregation of REEs into deposits enriched in either light lanthanides or heavy lanthanides plus yttrium (Castor et al., 2006; Steurer, 2017).

1.1.1 Occurrence of REE minerals

Geologically occurring compounds of REEs are in form of oxides, halides, carbonates, phosphates and silicates, but not sulfides. Although many minerals comprise of significant amount of REEs, their production has come from very few sources. This is because extraction and separation from a potentially economic REE resource is very much reliant on their nature of mineralogy. The major resources are primarily in four geologic environments: carbonatites, alkaline igneous systems, ion-adsorption clay deposits, and monazite-xenotime-bearing placer deposits (Jones et al., 1995; Kanazawa et al., 2006). While carbonatites and placer deposits are the sources

of producing light rare-earth elements, ion-adsorption clays are prospective sources for heavy rare earths (Voncken, 2016). The mineral deposits of REEs occur in a wide range of igneous, sedimentary and metamorphic rocks, wherein the concentration and distribution of the REEs in the minerals is influenced by numerous factors such as rock forming and hydrothermal processes (Habashi, 2013). Usually, the environments in which REEs are enriched are classified into primary deposits, associated with igneous and hydrothermal processes and secondary deposits, that are concentrated by sedimentary processes and weathering (Gupta and Krishnamurthy, 1992; Krishnamurthy and Gupta, 2015). The distribution of REE occurrences, deposits and mines in different parts of the world is shown in Figure 1.1.

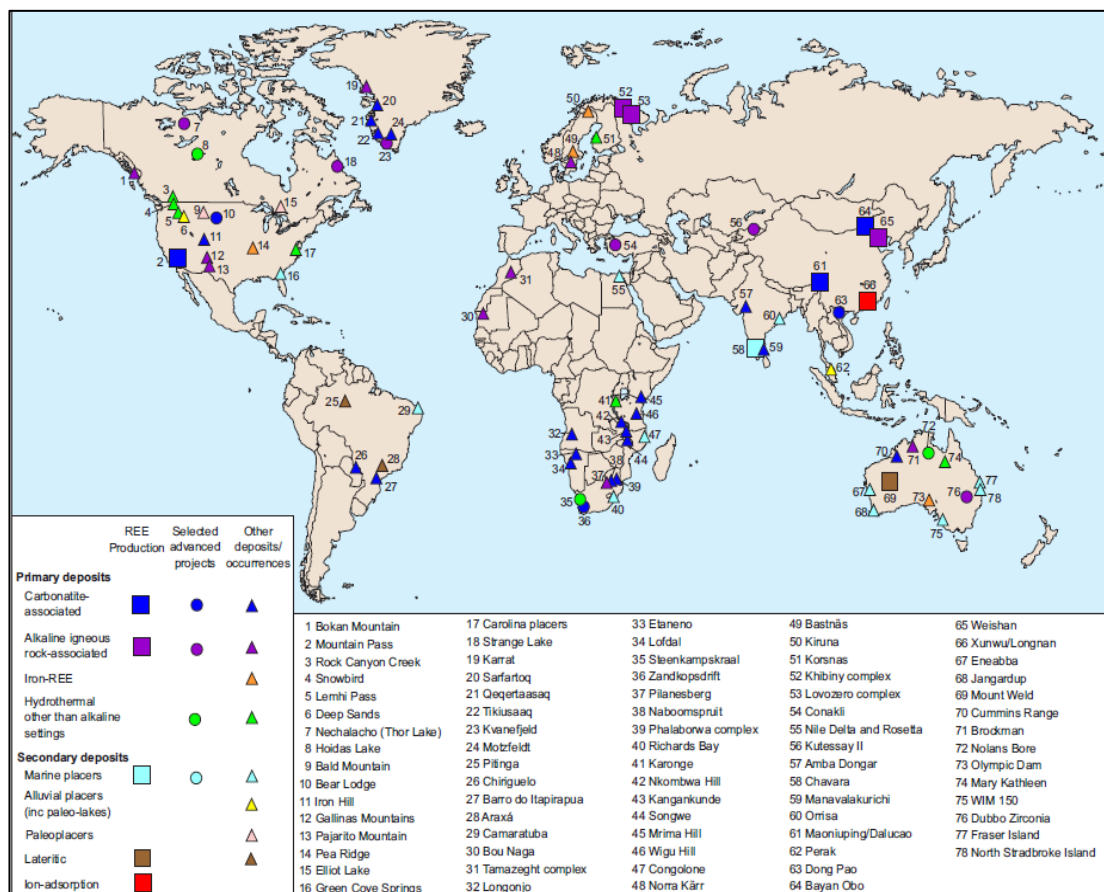


Figure 1.1 : Distribution of primary and secondary REE deposits across the globe (Walters et al., 2011). Based upon Mineral profiles on Rare Earth Elements, with the permission of the British Geological Survey

Most of the REEs are primarily found in carbonatites, which are igneous rocks composed of calcite (calcium carbonate), magnesium bearing carbonates (dolomite, magnesite) or siderites. Some of the alkaline igneous rocks, usually characterized by the high content of alkali metals. Apart from these, secondary deposits of REE, such as weathered primary sources subsequently concentrated by physical or chemical means i.e., placers or laterites are also a rich source of economically extractable REEs (Henderson, 1984; Migaszewski and Gałuszka, 2015). The proportions of different REEs vary between different deposits of the same mineral (Henderson et al., 2013). Some of the selected REE minerals and their corresponding approximate percent of rare earth oxides is given in Table 1.1.

Table 1.1: Selected major REE bearing minerals in the world (Estimates based on Web mineral composition (Barthelmy, 2007 ; Castor et al., 2006)

Mineral	Formula	Approximate REO %
Allanite-(Ce)	$(\text{Ce,Ca,Y})_2(\text{Al,Fe}^{3+})_3(\text{SiO}_4)_3\text{OH}$	32
Apatite	$\text{Ca}_5(\text{PO}_4)_3(\text{F,Cl,OH})$	19
Bastnasite-(Ce)	$(\text{Ce,La})(\text{CO}_3)\text{F}$	75
Britholite-(Ce)	$(\text{Ce,Ca})_5(\text{SiO}_4, \text{PO}_4)_3(\text{OH,F})$	32
Aeschynite-(Y)	$(\text{Ce,Ca,Fe,Th})(\text{Ti, Nb})_2(\text{O, OH})_6$	32
Fergusonite	$(\text{Ce,La,Nd})(\text{NbO}_4)$	53
Gadolinite	$(\text{Ce,La,Nd,Y})_2\text{FeBe}_2\text{Si}_2\text{O}_{10}$	60
Loparite	$(\text{Ce,La,Na,Ca,Sr})(\text{Ti,Nb})\text{O}_3$	30
Monazite-(Ce)	$(\text{Ce,La,Nd,Th})(\text{P,Si})\text{O}_4$	65
Xenotime	YPO_4	61
Florencite-(Ce)	$\text{CeAl}_3(\text{PO}_4)_2(\text{OH})_6$	32
Samarskite-(Y)	$(\text{Y,Ce,U,Fe}^{3+})_3(\text{Nb,Ti,Ta})_5\text{O}_{16}$	24

Thorium, one of the constituents of monazite, occurs in +4 state, together with uranium (IV), zirconium (IV), cerium (IV) as also with scandium (Sc), yttrium (Y) and other trivalent lanthanides that share similar ionic radii (Kizilyalli and Welch, 1976; Gupta et al., 1992) . The naturally radioactive nature of thorium makes the minerals

containing it metamict i.e., amorphous because the mineral structure is continuously subjected to damage by the alpha radiation produced by the radioactive element (Farges and Calas, 1991). Unlike uranium, thorium is fertile and not fissile by itself which makes it a safer replacement for U-238, which is fissile in nature (AL-Areqi et al., 2015; Lainetti, 2016). Thorium is a prominent member of several mineral groups such as monazite, allanite $(\text{Ce,Ca,Y,La,Th})_2(\text{Al,Fe}^{+3})_3(\text{SiO}_4)_3(\text{OH})$, and ekenite $(\text{Ca,Fe,Pb})_2(\text{Th,U})\text{Si}_8\text{O}_{20}$. It occurs as thorium dioxide (ThO_2) in the rare mineral, Thorianite and as thorite (ThSiO_4) (Cuthbert, 1958). The concentration of Th in different minerals is shown in Table 1.2.

Table 1.2: Thorium concentration ppm of various minerals (Wickleder et al., 2011)

Mineral	Th (ppm) range
Allanite-(Ce)	1000-20000
Monazite-(Ce)	25000- 2×10^5
Xenotime	low
Zircon	50-4000
Titanite	100-600
Epidote	50-500
Apatite	20-150
Magnetite	0.3-20

A reasonable concentration of REE bearing minerals that are economic to mine and with a profitable extraction process of REEs determine the exploitability of any particular mineral. A majority of minerals tend to be rich in both light and heavy REE's, including most of the REEs but in trace quantities. The deposits that are considered to be reserves will depend not only on fixed aspects like geographical distribution and concentration; mineral type, but also on variable factors such as commodity prices; regulatory regimes including environmental protection; improved technology for extraction and processing (Henderson et al., 2013; Balaram, 2019).

1.1.2 Principal REE minerals

The REE bearing minerals that have been extracted on a commercial scale are bastnaesite, monazite, and xenotime. Of all the minerals that contain the Naturally Occurring Radioactive Elements (NORE's), monazite and xenotime have gained widespread attention in the recent times (Krishnamurthy et al., 2015; Voncken, 2016). The two ubiquitous phosphate minerals, xenotime and monazite, can occur together, but crystallize in different temperature and pressure regimes from a similar igneous environment (Spear and Pyle, 2002). While monazite commonly occurs in placer deposits; xenotime can occur along with monazite, but generally occurs as a more minor constituent of these types of deposits (Overstreet, 1967). The mineral monazite is generally enriched with the REEs especially, lighter ones such as cerium, lanthanum, and neodymium, samarium, europium and gadolinium but can also contain HREEs, particularly yttrium (Ni et al., 1995; Zhu and O'Nions, 1999). Both the phosphate minerals usually also contain Th and/or U, but the amounts in monazite are subjective to be extracted as a valuable by-product based on their geological setting and concentration grade. Generally, studies revealed that REE ores of monazite are enriched with higher concentrations of thorium, and the heavy REEs in particular tend to concentrate in the same geological environments as thorium. Uranium also occurs in or with ore deposits that contain REE-bearing minerals. The concentrations of radioactive elements in the ore is not explicitly reliant on upon the mineral type, but more on the petrogenesis of the deposit containing the ore (Long et al., 2012). The disparity of xenotime to monazite and bastnaesite is that, the mineral generally contains, besides yttrium (Y), significant amounts of the HREE (Y, Tb, Dy, Ho, Er, Tm, Yb, and Lu). With respect to the actinides, monazite tends to concentrate thorium, whereas xenotime tends to concentrate uranium, but can also take up appreciable

amounts of thorium. Bastnaesite is another major REE ore mineral containing mostly the LREEs cerium, lanthanum, praseodymium, and neodymium and only Y, of the HREEs. Owing to the relatively lower concentrations of Th and U or absence of the two radioactive elements, the mineral has replaced monazite as a better source of LREEs. The mineral is primarily a carbonatite, with related minerals arising from substitution of the fluorine and carbonate ions (Krishnamurthy et al., 2015).

Monazite placer deposits, is an important source of REEs, used to be mostly abandoned because of its high thorium content. The environmental concerns related to radioactive elements and the association of REEs with thorium and uranium has demanded radiometric exploration techniques in REE exploration (Castor et al., 2006). Thorium and uranium represent the heaviest naturally occurring elements on Earth however, thorium is more abundant in nature than uranium. The inherent properties of Th has established the element to substitute U to be used to fuel a nuclear chain reaction that can run a power plant and make electricity however, thorium itself will not split and release energy which makes it fertile, whereas U-233 is called fissile (Lainetti, 2016). The huge energy needed by the nations, the advantages of thorium based fuel over uranium such as thorium resources which are several times larger than depleting uranium resources, and advantageous thermal and chemical properties and low actinide production in thorium based reactors are promoting thorium as a potential and relatively safe alternative for nuclear fuel (IAEA, 2005). The use of thorium as a new primary energy source has been a tantalizing prospect for many years yet extracting its latent energy value in a cost-effective manner remains a challenge and will require considerable research and development investment.

1.1.3 Malaysian monazite – Potential source of REEs and Thorium

The rare earth production in Malaysia is usually from two REE- bearing minerals, monazite and xenotime. The abundant cassiterites present in the alluvial tin deposits in Malaysia occur with several other minerals such as ilmenite, monazite, xenotime, and zircon. The cassiterite and other associated minerals usually occur as free grains liberated from the primary ore body. Malaysia has several minerals (e.g. monazite, zircon, xenotime and ilmenite) which are categorized as strategic minerals because they contain an amount of thorium and uranium with the total concentrations of uranium and thorium above 500 ppm which requires a regulatory control (Lainetti, 2016). The average range of thorium content in Malaysian monazite and xenotime minerals was found about 70,000 and 15,000 ppm respectively (Omar, 2010). Studies revealed that, from the year 2006 until 2010, about 2,636 tonnes of Malaysian monazite was produced. Based on this data, it can be estimated that Malaysian monazite contains about 184.5 tonnes of thorium. Although thorium can become a major radiological problem to our environment, but with the significant deposit of thorium in Malaysian monazite, it has a prospect as a future alternative fuel in nuclear technology (AL-Areqi et al., 2015).

Monazite, being a more common mineral of occurrence in this region, is separated as a byproduct from cassiterite ores along with silica, magnetite, ilmenite, zircon and garnet. The concentration of monazite is accomplished by using washing and electromagnetic separation, which separate monazite from other minerals by their different magnetic permeabilities. Thorium is mainly obtained from monazite sands as a by-product of extracting rare earth metals (Sulaiman, 1991). Nevertheless, in the case of thorium, the rare earths will be mined anyway and the tails containing thorium can be used without the generation of additional wastes. Then, it was not necessary mining

thorium, since it will be available anyway as a side product of the rare earth industry. This avoids big problems related to the mining industry, mainly from the environmental point of view. With an estimated reserve of 30,000 tons of rare earth mineral reserves by Sanusi et al. (2017), Malaysian monazite was composed of 6.5-7.5 wt. % of Th and 55.5-75.5 wt. % of REOs (ASM, 2013; AL-Areqi et al., 2015) . Significant amounts of Th can also be separated from rare earth residue of rare earth elements industries as it causes considerable concern on their proper management to avoid radioactive pollution and contamination of rare earth products (IAEA, 2005).

1.2 Problem statement

For the past ten years, much effort has been expended by several research teams to develop an economic process for recovering thorium, rare earths and uranium from monazite sands (Omar, 2010; Al-Areqi et al., 2014; AL-Areqi et al., 2015). In Malaysia, it was possible to produce thorium from two main sources: Monazite and old RE residues, containing 36 wt. % of ThO₂, generated from monazite processing after extracting rare earth elements. Separation of thorium from the residue using the multi-stage process will reduce the hazard of radioactivity and obtain thorium oxide for future use in nuclear energy. Despite consistent efforts and attempts by the scientific community to establish a safe, economic and reliable concept of separation of the naturally occurring radioactive elements (NORE) like thorium and uranium there are a lot of practical issues in executing process as such. This is because of the need for more caution and care in handling the experimental residues, elements and the surroundings (Sulaiman, 1991). From literature review, researchers have briefly classified monazite and described their variations with respect to the composition and physical characteristics for different geological environments (Bashir, 1988; Abdel-Rehim, 2002; Panda et al., 2014; Sadri et al., 2017; Udayakumar et al., 2018).

However, there is sparse information or lack of inclusive evidence on the mineralogical and chemical characteristics of monazite, particularly originated from peninsular Malaysia, despite Malaysia bearing rich deposits of the rare earth phosphate mineral.

Currently, the prevailing state of the art processes for REE and Th extraction from monazite follows complicated and resource and energy-intensive technologies for production of REE and Th rich concentrate (Peelman et al., 2015). The extraction and recovery process of the REEs and thorium commenced from the physical beneficiation followed by leaching, purification and separation into individual compounds and refining to produce high purity RE metals (Jordens et al., 2013; Kumar et al., 2014; Kumari et al., 2015; Verbaan et al., 2015; Zhu et al., 2015; Sadri et al., 2017). The extractive metallurgy of REEs from monazite involves decomposition of rare earth mineral, and the subsequent leaching of the rare earth elements from the minerals. Usually the beneficiated concentrate was decomposed, for example, by acid roasting, caustic cracking, and mechanical methods and the REEs can be selectively extracted (Bahri et al., 2016; Borai et al., 2018; McNeice and Ghahreman, 2018). The nature of the rare earth extraction process depends on the type of minerals in the concentrate, the grade of the concentrate and the targeted products (Zhu et al., 2015).

Various hydrometallurgical processing routes using sulfuric, nitric and hydrochloric acid and alkaline reagents have been investigated and established by researchers for recovering rare earths from monazite and xenotime (Bridger et al., 1951; Moore et al., 1957; Abreu and Morais, 2010; Amaral and Morais, 2010; Kim et al., 2014; Stone et al., 2016). A comprehensive review of the preliminary cracking and leaching methods applied to produce REE concentrates have been presented elsewhere (Sadri et al., 2017). Apart from the above mentioned industrially practiced methods,

the literature has also proposed methods like high temperature reduction (Merritt, 1990a; Merritt, 1990b; Pengfei et al., 2010; Xing et al., 2010) and roasting (Zheng et al., 2017a; Zheng et al., 2017b), mechano-chemical decomposition (Kim et al., 2009) and other independent methods (Ha, 1979; Zhang and Lincoln, 1994; Yanhui et al., 2012; Huang et al., 2016; Berry et al., 2017)

The processing of monazite imposes a lot of challenges to extractive metallurgist as the mineral is a complex system of several light rare earths in a solid solution of orthophosphates. In case of monazite in the current study, which has a rare earth composition of ~60 wt.%, during the extractive metallurgical process, there are possibilities of phosphide formation which may permeate into the end products affecting their functionality. The nature of decomposition is decided based on the characteristics of the mineral concentrate including their mineralogical composition and chemical reactivity. In order to cater to all aspects of the technical and environmental concerns, it is essential to engage in a sustainable method of extractive metallurgy based on the mineralogy. From this perspective, there exists a definite need to understand the kinetics and thermodynamics of the processing system which suits the mineralogy of the monazite concentrate in hand. The development of a leaching model that can predict both recovery and reagent consumption using available mineralogical data will help reduce the costs and time of processing. The envisaged model will be used as a tool for predicting hydrometallurgical routes.

Several leaching methods were studied and industrially applied for the breakdown of the principal REE minerals. However, there was a need to shed some light on the kinetics of the leaching reactions which is essential for the industrial reliance for sustainable production of REEs to cater diverse applications. Since Malaysia has a rich source of REE's and thorium, and a significant number of REE

industries and a national nuclear research institute (Malaysian Nuclear Agency), there is an opportunity for Malaysia to exploit the abundant thorium from monazite for establishing a safe and consistent energy generation system. By pursuing the thorium fuel cycle, Malaysia will be able to create cleaner REE industries (free of thorium waste) and a sustainable energy system for the near and far future. The current research will also be a basis to develop thermodynamic models for separating the rare earths and thorium obtained by leaching the ore. This research, in particular, will serve as the forerunner in the separation of the REE elements from their Malaysian monazite ores through an innovative alkaline fused acid-leach method. This approach is expected to directly impact on product and process performance, and ultimately bring about corporate profitability.

1.3 Objectives of the study

The main objective of this research was to develop a sustainable and environmental-friendly method for recovering the rare earth elements and thorium from Malaysian monazite. The specific objectives of this research are:

- (i) To examine the mineralogy, chemical composition, morphology, size distribution, phase analysis, and thermal behavior of Malaysian monazite concentrate by using different characterization methods.
- (ii) To evaluate the thermodynamics of decomposition and dephosphorization behavior of Malaysian monazite and study the effects of different carbothermal reduction parameters such as temperature, reduction time, particle size in the formation of the rare earth and thorium oxides using statistical design of experiments (DOE) i.e., Taguchi method.

- (iii) To investigate the thermodynamics of alkaline fusion and acid leaching reactions for monazite and to determine the best conditions for the alkaline fused-water leaching of monazite and the acid leaching of the RE and Th hydroxides and oxides for high-efficient recovery of the constituent rare earths and thorium using fractional factorial design of experiments (FFD).

1.4 Scope of the research

In spite of the development of diverse techniques to recover REE's and Th from monazite, there was a need to select the most appropriate beneficiation and leaching method based on the unique mineralogy of the ore. Each rare earth deposit is unique depending on their source and geography of formation; thus, the composition of monazite varies among different locations. It is not efficient in terms of recovery and effective in terms of the process to apply similar recovery process established for minerals with varying characteristics and complexities of mineralogy. Furthermore, the detailed analysis of the composition of Malaysian monazite will be useful to be compared with global trends to evaluate the viability for commercial exploitation of the mineral. For an efficient recovery of the REE's from Malaysian monazite, the current study's aim was to understand the mineralogy, chemical composition, surface functional groups, particle size, morphology and thermal stability through in-depth characterization. The knowledge gained on the mineralogy, associated impurity phases, liberation analysis and decomposition behavior will be a prerequisite to understand and predict the behavior of the mineral constituents to different beneficiation routes.

The ultimate goal was to characterize chemically and mineralogically, investigate the decomposition behavior of Malaysian monazite under the proposed carbothermal and pyro-hydrometallurgical route. It is worthwhile to note that

efficiency of the recovery process is influenced by several factors- essentially the thermodynamic and kinetic factors apart from the chemical process employed in the process. Therefore, the thermodynamic analysis of the reaction system (Sections 4.3.1, 4.4.1 and 4.7) was performed which served as a basis for prediction of the reaction routes of the individual components (rare earths and thorium) in the system. The alkaline fusion of Malaysian monazite and acid leaching of the RE and Th hydroxides and oxides were comprehensively studied using statistical design of experiments (DOE) in this research. The current study will be an eye-opener in the domain highlighting the need to investigate, better operating conditions to optimize REEs and thorium extraction, and to develop suitable modeling tools to assess and diagnose the leaching performance.

1.5 Organization of thesis

The thesis was organized in five chapters. The brief summary on the chapters are described as follows:

- i) Chapter One includes a short introduction on rare earth elements and thorium production, world reserves of monazite and a summary of the different metallurgical processes currently in use for recovering the constituent elements from monazite is included. Also, the objectives, scope of the research study and the key challenges of the thesis is presented in Chapter One.
- ii) Chapter Two contains a survey of the research background and relevant literature review on hydrometallurgical and pyrometallurgical processing of monazite.
- iii) Chapter Three describes the experimental procedure, set-up and the equipment employed, and the information on the design of experiments used to conduct this research.

- iv) Chapter Four presents the results and discussion on the characterization of Malaysian monazite. The characterization study was followed by the results of the proposed pyrometallurgical process. The effect of different factors of the carbothermal reduction on the dephosphorization efficiency of the mineral was statistically investigated supported by chemical and microstructural analyses. The results of the alkaline fused acid-leached process have also been narrated in detail with calculation of recovery of the constituent REEs and Th in monazite. The research also proposes and successfully examined a method of modified acidic leaching for improving the low recovery obtained during acid leaching.
- v) In Chapter Five, conclusions of the research work, recommendations and suggestions for future work on this field of processing monazite for recovering of REEs and Th are presented.

CHAPTER TWO

LITERATURE REVIEW

2.1 Introduction

This chapter provides an exhaustive and chronological information on different processing routes of monazite for recovering their constituent REEs, Th and U. Firstly, the occurrence and association of the mineral monazite in different environments is elucidated. The different sources of monazite in the world, their production statistics in Malaysia and other parts of the world is narrated. The next section of this chapter briefs on the various applications catered by the REEs and Th, particularly the constituent elements of monazite. The second part of this chapter concentrates on the decomposition methods that have been used in the past, at present in laboratory and commercial scale. The pyrometallurgical and other non-conventional methods of processing monazite are reviewed. The current available methods of separation and purification of the rare earth elements and Th, U from their aqueous solutions have been briefly outlined. The rare earth ore beneficiation, mineral concentrate decomposition, and rare earth leaching are introduced briefly. An overview on the various hydrometallurgical flowsheets of monazite processing i.e., acidic and alkaline leaching is provided. The literature in various databases and websites have been compiled and analyzed critically. The key literatures were identified, and data were compiled from these openly available materials. Then, the kinetic factors affecting the leaching process that have been studied so far by various researchers are compared, and peculiar attributes of the factor are discussed in detail in relation to the current work. The final part of the chapter details on the Design of Experiments (DOE) methods employed for conducting experiments. The advantages and disadvantages of the Taguchi, Factorial and Fractional design of experiments have been reviewed.

2.2 Geological occurrence of monazite

Monazite is widely distributed throughout the world as a minor accessory mineral in intermediate- and high-rank metamorphic rocks derived from argillaceous sediments (Bashir, 1988). Monazite is less commonly present in metamorphic rocks of like facies formed from arenaceous sediments and is rarely present in metamorphosed calcareous sedimentary rocks (Overstreet, 1967). The mineral is especially common in argillaceous schists, gneisses, and migmatites of the upper sub-facies of the amphibolite facies and of the granulite facies. Monazite occurs in magmatic rocks ranging in composition from diorite to muscovite granite, and in associated pegmatite, greisen, and vein quartz (Gillson, 1960).

Carbonatite, a rare igneous rock, contains the highest REE concentrations of any of the igneous rocks, and is especially enriched in LREE. The three most important REE minerals in carbonatite related deposits are bastnasite, monazite, and xenotime (Chen et al., 2017), and are also the only REE bearing minerals that have been extracted on a commercial scale. Monazite is similar to bastnasite as a LREE ore mineral, but with slightly more HREE (Spear et al., 2002). Monazite, together with niobate, fluorocarbonate and apatite, serve as the most useful carbonatite indicator minerals for specialty metal exploration. The secondary monazite commonly shares mineral associations with apatite, barite, fluorite, hematite, quartz, sulfide, bastnasite, xenotime, feldspar, titanite, synchysite, goyazite, and strontianite (Migaszewski et al., 2015).

2.3 Distribution of monazite sources in the world

The mineral monazite is a thorium-bearing anhydrous phosphate of the cerium earths. The mineral is a major source for thorium, with an average 6 wt. % in most of the sources. Monazite and bastnaesite, a fluorocarbonate of the lanthanide earths, are the main ores for the cerium group of the rare earths. Monazite is distributed throughout the world in a wide variety of geologic environments. Most commonly it occurs as an accessory mineral in Precambrian gneisses, schists, and migmatites. Monazite deposits in Asia include the world's largest known reserves, which are in the coastal deposits of India, and the world's most thorium-rich monazite deposit, which is mined in Ceylon. The resources of monazite in stream and beach placers of India, southeast Asia, and Korea seem to be immense. The commercial exploitation hinges on beneficiation of multimineral concentrates in which monazite is associated with ilmenite, rutile, cassiterite, wolframite, and gold. Although abundant in the tin and tungsten placers of eastern Australia, monazite has been commercially unacceptable because it generally contains less than 2 wt. % of ThO₂. Large resources of monazite have been discovered in fossil placers that range in age from Precambrian to Late Cretaceous. Very large low-grade resources of monazite doubtless exist with ilmenite in the sedimentary rocks of the Atlantic and Gulf Coastal Plains and in offshore deposits of the Southeastern United States and the gulf coast of Mexico. Marine beaches and elevated bars along the southern coast of Brazil were the world's main source of commercial monazite during the 1960-80's (Overstreet, 1967; Krishnamurthy et al., 2015).

Thorium can usually be present as anhydrous phosphates or oxides in monazite and the amount was variable (4-12 wt. %) depending on the mineralogical origin of the ore (Habashi, 2013). Majority of monazite mining is concentrated on placer

deposits because of the ease of mining and their higher concentrations than in hard rock deposits. Other heavy minerals that accumulate with monazite include magnetite (Fe_3O_4), ilmenite (FeTiO_3), rutile (TiO_2), zircon (ZrSiO_4), cassiterite (SnO_2), wolframite ($(\text{Fe,Mn})\text{WO}_4$) and a variety of gemstones. The combined occurrence of the heavy elements in rare earth minerals like monazite and xenotime can be attributed to their high specific gravity (4.5-5.5) and resistance to weathering and erosion as a result of which they concentrate along the coast by tidal waves and coastal winds to form onshore and offshore placer deposits (Overstreet, 1967; Bashir, 1988).

2.3.1 Monazite: Global production

Rare earth minerals like monazite, xenotime and bastnaesite have become a valuable source for variety of REE's, especially in the field of advanced materials, green energy technology and electronics. Although the distribution of REE's is not homogenous, yet globally widespread, the production is largely monopolized by China. Monazite, being an important REE mineral source in the world is concentrated in several countries: China, India, Malaysia, Sri Lanka and Australia (Ober, 2018). Other countries that mine and produce REE's are USA, Australia, Canada, South Africa and Brazil (Hedrick, 2004; Castor and Hedrick, 2006). Table 2.1 provides a comparison of the distribution of REOs in monazite from the tailings of Ipoh, Malaysia with mines in the world.

Table 2.1: Comparison of rare earth fraction and thorium concentration in monazite from different locations

Source of monazite	Average content of REEs (wt. %)	Average content of Th (wt. %)	Reference
Alinci, Yugoslavia	65	3.5	Bermanec et al., 1988.
Siberia (Tomtor)	10.2	-	Kuzmin et al., 2012.
Siberia (Chuktukon)	7.1	-	Kuzmin et al., 2012.
Iran	24.7	0.2	Sadri et al., 2017.
Egypt	62.41	6-6.5	Abdel-Rehim, 2002; El-Nadi et al., 2005.
India (Chavara, Manavalankurichi)	55-60	5-7	Bashir, 1988; Lal et al., 1989.
Western Australia	55-58	6-7.5	Jaireth et al., 2014.
China (Beihai Processing plant)	60-63	6.3	Krishnamurthy et al., 2015.
Korea	60-70	-	Panda et al., 2014.
South Africa	48-50	6.8	Kemp, 2017.

The reasonable concentration of thorium associated with the REE's has increased the interest of mineralogists worldwide to engage in geological surveys to fulfill the anticipated global demands for thorium in the upcoming years. The similarities in the crystal structure of Th and U with rare earths are the reason they occur as lattice substitutions in the mineral monazite thus, raising concerns of waste management in rare earth processing of these minerals (Kanazawa et al., 2006; Haque et al., 2014). A high global demand and strained supply was resulted due to the reduction in the supply quotas of REE minerals, thus creating opportunities for other countries with reasonable amounts of the minerals to look into self-sufficient sources (Moila et al., 2017).

2.3.2 Monazite production in Malaysia

Malaysia has several minerals (e.g. monazite, zircon, xenotime and ilmenite) which are categorized as strategic minerals because they contain an amount of thorium and uranium with the total concentrations of uranium and thorium is above 500 ppm which requires a regulatory control (Omar, 2010). Usually, thorium exists in minerals and rare earth elements production residue. The average range of thorium content in Malaysian monazite and xenotime minerals was found about 70,000 and 15,000 ppm respectively (Sulaiman, 1991; AL-Areqi et al., 2015). About 2,636 tonnes of Malaysian monazite was produced for a period of 5 years (2006-2010) and based on this data, it can be estimated that Malaysian monazite contains about 184.5 tonnes of thorium. Although thorium can become a major radiological problem to our environment, but with the significant deposit of thorium in Malaysian monazite, it has a prospect as a future alternative fuel in nuclear technology (Sulaiman, 1991; Omar, 2010; AL-Areqi et al., 2015).

Malaysia has been producing monazite and xenotime for the last few decades but, the amounts of production have been fluctuating yearly, as can be seen in Table 2.2 (Malaysian Minerals Yearbook, 2017). A major portion of monazite is produced with xenotime as byproducts of tin mine processing (Amang plant) in Malaysia (Sulaiman, 1991; Omar, 2010). With an estimated reserve of 30,000 tons of rare earth mineral reserves (Sanusi et al., 2017), Malaysian monazite is composed of 6.5-7.5 wt. % of Th and 55.5-75.5 wt. % of REOs (IAEA, 2005; 2013). Significant amounts of Th can also be separated from rare earth residue of rare earth elements industries as it causes considerable concern on their proper management to avoid radioactive pollution and contamination of rare earth products (Al-Areqi et al., 2014; 2015).

Table 2.2: Production of rare earth minerals in Malaysia from 2014-17 (in metric tons) (Malaysian Minerals Yearbook, 2017)

Commodity produced	2013	2014	2015	2016	2017
Industrial minerals:					
Rare earths, monazite and xenotime, gross weight	358	946	565	1880	302

2.3.1 World reserves and production of REEs

An accurate figure for quantifying the global rare earth resources has not been possible owing to the quality and availability of accessible data. Based on the mineral commodity summaries annual report published by USGS in early 2019, the estimated total world reserves of rare earth oxides are about 120 million tonnes (USGS, 2019).

Table 2.3 : Estimated world mine production of rare earth oxides and reserves (USGS, 2019)

World Mine production and reserves (in tonnes)			
Country	Estimated mine production		Reserves
	2017	2018	
Unites States	-	15,000	140,000
Australia	19,000	20,000	340,000
Brazil	1,700	1,000	22,000,000
Burma	Not available	5,000	NA
Burundi	-	1,000	NA
China	105,000	120,000	44,000,000
India	1,800	1,800	6,900,000
Malaysia	180	200	30,000
Russia	2,600	2,600	12,000,000
Thailand	1,300	1,000	NA
Vietnam	200	400	22,000,000
Other countries	-	-	4,400,000
World total (rounded)	132,000	170,000	120,000,000

Table 2.3 gives the estimated world mine production of rare earth oxides. China dominates the world reserves with 36 percent, followed by Brazil and Vietnam with 18 percent, Commonwealth of Independent states (CIS) with 10 percent, India with 6 percent, Australia with 3 percent, United states with 1.5 percent and remaining divided

among Canada, Malaysia, Sweden, Finland South Africa, Namibia, and Thailand., REEs have been marketed in a variety of products ever since their first venture of capitalization. Industries and mineral processing companies are also taking a renewed interest in REE commercialization, as increased prices (and in some cases government incentives) make exploitation of resources potentially more profitable. Also, the advances in the processing flowsheets have brought the possibilities of bringing the applicability and availability of REEs closer. In recent years, the novel properties of rare earth elements have attracted burgeoning interests from the research community towards diversifying the range of applications, especially in low-carbon technologies, high-strength permanent magnets, catalysts for petroleum refining, metal and glass additives and phosphors used in electronic displays (Zhou et al., 2017).

In recent decades, rare earths have become an indispensable aspect to a wealth of advanced materials and technologies including alloys, optics and lasers, rechargeable hydride batteries, electronics, economical lighting, wind- and solar-energy conversion, bio-analyses and imaging and have been termed as “jewels for functional materials of the future”. From Figure 2.1, it can be seen that REEs have been exploited in potentially dedicated applications telecommunications, lasers, photovoltaics (solar-energy conversion), lighting (fluorescent lamps and OLEDs), luminescent probes for bio-analyses and bio-imaging, as well as magnetism and magnetic refrigeration (Eliseeva and Bünzli, 2011). The REEs are used in two forms in most of the applications namely; "Mischmetall", a mixture of rare earth oxides and "high purity" compounds containing at least 90% of an individual rare earth element (Preinfalk and Morteani, 1989). The prospects to broaden the applications of REEs will continue to be of extensive interest for the foreseeable future, with more demand likely to grow.

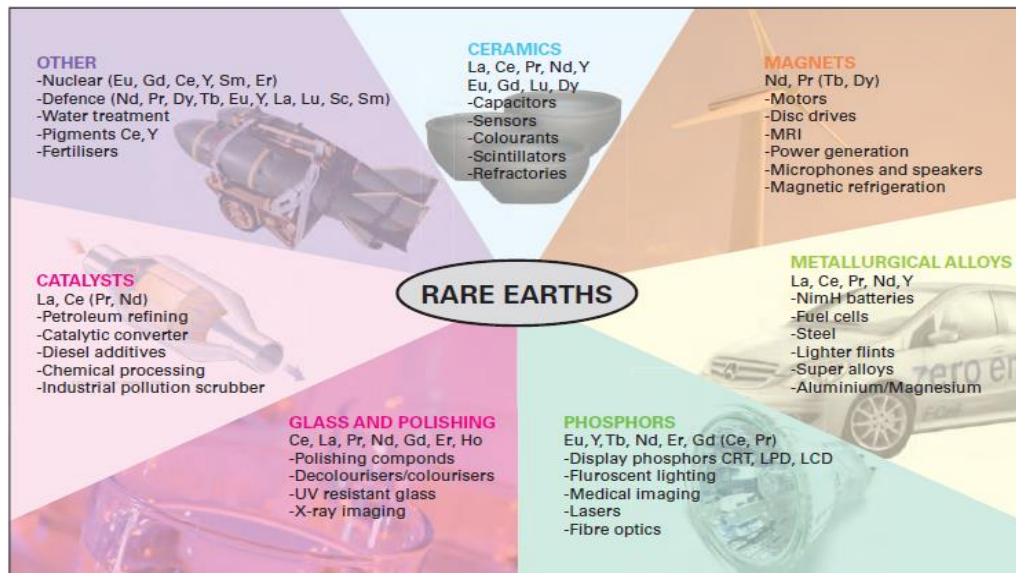


Figure 2.1: Diversity of applications of Rare Earth Elements. Image courtesy of Mercedes-Benz, Matthey Plc and Ingrey Publishing

2.4 Mineralogical variations of monazite

Several researchers have reported on the mineralogical characteristics of monazite from various sources prior to the physical or physiochemical processing of the ore. Studies on Iranian monazite showed that the concentrates accumulated in the fine size fraction (< 2mm) and the major mineral phases identified were monazite (consisting of La, Ce and Nd compounds), quartz and augelite ($\text{Al}_2(\text{PO})_4(\text{OH})_3$) (Sadri et al., 2017). The liberation analysis confirmed the existence of liberated grains of hematite, gray monazite and rarely magnetite and quartz. The Rosetta monazite concentrate from Egypt was characterized by high rare earth phosphate content about 57 wt. % and relatively low Fe_2O_3 , SiO_2 and TiO_2 contents reaching about 3.00, 2.80 and 2.80 wt. % respectively (Amer et al., 2013). On the other hand, the studies on the mineral chemistry of monazite from black sands of northern Sinai, Egypt revealed two distinct types of the mineral namely, monazite-(Ce) and Th-rich monazite. While the study indicated that monazite-(Ce) was more enriched in REE and P, Th-rich monazite was more enriched in Th, Ca, Si, Y, U and Fe (Dawood and El-Naby, 2007). A study by